Geophysical Research Letters

RESEARCH LETTER
10.1029/2023GL106772

Can Glacial Sea-Level Drop-Induced Gas Hydrate Dissociation Cause Submarine Landslides?

Jinlong Liu[1], Shubhangi Gupta[2,3], Jonny Rutqvist[4], Yikai Ma[5], Shuhong Wang[1], Kuiyuan Wan[1], Chaoyan Fan[1], and Wen Yan[1,6]

[1]Key Laboratory of Ocean and Marginal Sea Geology, South China Sea Institute of Oceanology, Innovation Academy of South China Sea Ecology and Environmental Engineering, Chinese Academy of Sciences, Guangzhou, China, [2]GEOMAR Helmholtz Centre for Ocean Research Kiel, Kiel, Germany, [3]Department of Geosciences, University of Malta, Msida, Malta, [4]Lawrence Berkeley National Laboratory, Berkeley, CA, USA, [5]South China Sea Standards and Metrology Center of State Oceanic Administration, Guangzhou, China, [6]University of Chinese Academy of Sciences, Beijing, China

Abstract We conducted two-dimensional numerical simulations to investigate the mechanisms underlying the strong spatiotemporal correlation observed between submarine landslides and gas hydrate dissociation due to glacial sea-level drops. Our results suggest that potential plastic deformation or slip could occur at localized and small scales in the shallow-water portion of the gas hydrate stability zone (GHSZ). This shallow-water portion of the GHSZ typically lies within the area enclosed by three points: the BGHSZ–seafloor intersection, the seafloor at ~600 m below sea level (mbsl), and the base of the GHSZ (BGHSZ) at ~1,050 mbsl in low-latitude regions. The deep BGHSZ (>1,050 mbsl) could not slip; therefore, the entire BGHSZ was not a complete slip surface. Glacial hydrate dissociation alone is unlikely to cause large-scale submarine landslides. Observed deep-water (much greater than 600 mbsl) turbidites containing geochemical evidence of glacial hydrate dissociation potentially formed from erosion or detachment in the GHSZ pinch-out zone.

Plain Language Summary Many submarine landslides spatiotemporally correlate with gas hydrate dissociation. However, direct mechanical evidence supporting whether the overpressure and deformation due to glacial sea-level drop-induced hydrate dissociation are adequate for triggering submarine landslides is lacking. Here, we present two-dimensional thermal-hydraulic-chemical and geomechanical models of a gas-hydrate system in response to glacial sea-level drops and conduct sensitivity analyses of the model behavior under a wide range of key conditions from a global perspective. Our simulations suggest that glacial hydrate dissociation might induce plastic deformation or slip at localized and small scales only possibly within the shallow-water portion of the hydrate stability zone. The deep part (>1,050 m below sea level) of the bottom boundary of the hydrate stability zone could not slip; therefore, the entire bottom boundary of the hydrate stability zone was not a complete slip surface. We demonstrate that glacial hydrate dissociation alone is unlikely to trigger large-scale submarine landslides. Our work highlights the vicinity of the upper limit of the hydrate stability zone (where the base of the hydrate stability zone intersects the seafloor) as an important area for investigating overpressure and focused fluid flow, localized plastic deformation or slip, and downslope sediment transport related to glacial hydrate dissociation.

Key Points:

- Glacial hydrate dissociation might cause potential plastic deformation or slip at localized and small scales in shallow parts of the GHSZ
- The large deformation surface at the BGHSZ boundary of the potential plastic deformation zone was not a complete slip surface
- Glacial sea-level drop-induced gas hydrate dissociation alone is unlikely to have caused large-scale submarine landslides

Supporting Information:

Supporting Information may be found in the online version of this article.

Correspondence to:

S. Wang,
wshds@scsio.ac.cn

Citation:

Liu, J., Gupta, S., Rutqvist, J., Ma, Y., Wang, S., Wan, K., et al. (2024). Can glacial sea-level drop-induced gas hydrate dissociation cause submarine landslides? *Geophysical Research Letters*, *51*, e2023GL106772. https://doi.org/10.1029/2023GL106772

Received 18 OCT 2023
Accepted 2 MAR 2024

Author Contributions:

Conceptualization: Jinlong Liu, Yikai Ma
Data curation: Shuhong Wang
Formal analysis: Jinlong Liu, Shubhangi Gupta, Jonny Rutqvist
Funding acquisition: Shuhong Wang, Wen Yan
Investigation: Yikai Ma
Methodology: Jinlong Liu, Shubhangi Gupta, Jonny Rutqvist
Project administration: Kuiyuan Wan, Chaoyan Fan
Resources: Kuiyuan Wan, Chaoyan Fan, Wen Yan
Validation: Jonny Rutqvist
Visualization: Shubhangi Gupta

1. Introduction

Many submarine landslide scars are found in gas hydrate fields, and the ages of some slides show a temporal correlation between increased slumping frequency and the last glacial sea-level lowstands. Known examples are found at the southern Carolina Rise and inner Blake Ridge (Paull et al., 1996); at the Amazon Fan (Maslin et al., 1998); and at the Dongsha area of the northern South China Sea (Huang et al., 2022). A glacial sea-level drop could induce a decrease in pore pressure, and if the gas hydrate stability zone (GHSZ) thinning due to pore pressure decreases overwhelms the trend of GHSZ thickening due to glacial temperature decreases, this process could induce hydrate dissociation at the base of the GHSZ (BGHSZ). Hydrate breakdown can reduce sediment cohesion (Liu et al., 2018), and the occurrence of free gas in the intergranular space due to hydrate dissociation can increase pore pressure and reduce the shear strength of sediments (Locat & Lee, 2002). Therefore, glacial hydrate dissociation can degrade slope stability (Paull et al., 2003) and has been predicted to be the cause of some submarine landslides during glacial periods (Maslin et al., 2005; Owen et al., 2007).

Writing – original draft: Jinlong Liu
Writing – review & editing: Shubhangi Gupta, Jonny Rutqvist, Yikai Ma, Shuhong Wang, Kuiyuan Wan, Chaoyan Fan, Wen Yan

Since the early 2000s, scientists have investigated whether hydrate dissociation can induce slumping via numerical modeling studies. In one-dimensional models (Handwerger et al., 2017; Liu & Flemings, 2009), the heat and mass transfer, which influence overpressure accumulation, and geomechanical deformation in the lateral direction (i.e., at different water depths along the slope) are not considered. In two-dimensional geomechanical models, overpressure is either not calculated from the heat and mass balance equations for the gas, pore water and hydrate system (Nixon & Grozic, 2007) or is estimated from ocean warming-induced hydrate dissociation (Priest & Grozic, 2016; Reagan et al., 2011; Sultan et al., 2004). The two-dimensional geomechanical deformation caused by the overpressure generated by dynamic hydrate dissociation due to glacial sea-level drops was not the primary focus of these numerical studies and has not been adequately evaluated.

Here, we present numerical simulations to investigate whether glacial hydrate dissociation can induce submarine landslides. We consider overpressure generation due to glacial hydrate dissociation with pressure-induced triggering of landslides along localized plastic shear slip planes. We use the geological setting of the Dongsha area in the northern South China Sea in low-latitude regions (Figure 1a) as a case study because of several key features allowing us to investigate links between hydrate dissociation and submarine landslides. First, turbidite deposits are present between 4.47 and 6.01 m below the seafloor (mbsf) (Figure 1b), with temporal consistency between the initial time of upper slope slumping (17.93 ka) (Figure 1g) and the occurrence of a global sea-level lowstand during the last glacial period (Miller et al., 2020) (Figure 1h). Moreover, there is a record of potential methane emissions from hydrate decomposition within or beneath the turbidite deposit, as indicated by the heavier $\delta^{18}O$ and lighter $\delta^{13}C$ values of the benthic foraminifera *Uvigerina* spp (abbreviated for several species) and heavier $\delta^{34}S$ values of chromium-reducible sulfur before the end of the Last Glacial Maximum (Figure 1c–1f). Our simulations present systematic and direct fluid dynamics and geomechanical evidence for the links between glacial hydrate dissociation and submarine landslides.

2. Methods

Hydrate dissociation, fluid flow and thermal behavior in the gas hydrate system were simulated using the parallel version of the TOUGH + HYDRATE code with the kinetic hydrate reaction model (Moridis, 2014). At the end of the calculation, the pore pressure was imported into the FLAC3D geomechanical simulator to compute the deformation with the Mohr–Coulomb elastoplastic mechanical model.

The model system is a two-dimensional slice of a slope in the upper shallow-water area of Sites 973–3 (1,026 mbsl) and 973–4 (1,666 mbsl) (Figures 1a and 1i). The model geometry is shown in Figure 1i, and the z coordinates are in meters below current sea level (mbsl). The model is presented in detail in Text S1 in Supporting Information S1. The supplementary model parameters and equations used are listed in Table S1 in Supporting Information S1.

3. Results

The main simulation results are presented for two scenarios. In subsection 3.1, the sea level decreased by 65.22 m from 35 to 20 ka (4.38 m/kyr on average), and the changes in sea level and seafloor temperature were the same as those measured at ODP Site 1,148 (Bates et al., 2014) (Figure 1a), as shown by the red line and blue line in Figure 1h. In subsection 3.2, it was assumed that the sea level decreased by 138.7 m at a rate of 8.0 m/kyr and that there was no change in seafloor temperature. This assumption may lead to a slight overestimation of hydrate dissociation since the seafloor temperature generally decreases during glacial periods. Therefore, this assumption will not underestimate the likelihood of glacial hydrate dissociation inducing slope failure. The value of 138.7 m represents the maximum sea-level decrease from the last interglacial highstand (+8.7 m at 124 ka) to the last glacial lowstand (−130 m at 20 ka) (Bates et al., 2014). The value of 8.0 m/kyr is lower than the maximum sea-level decrease rate (13.8 m/kyr from 47.3 to 45.7 ka), close to the second (8.23 m/kyr from 81.8 to 72.6 ka) and third (8.18 m/kyr from 24 to 20 ka) highest decrease rates, and greater than the average decrease rate between 124 and 20 ka (1.33 m/kyr) (Bates et al., 2014).

3.1. The Sea Level Drop of 65.22 m From 35 to 20 ka

The hydrate saturation decreased in one of two ways: dissolution or dissociation (Figures 2a or 2e). When the pressure–temperature–salinity conditions are suitable for stable hydrates, dissolution occurs when hydrates come into contact with ocean water or pore water undersaturated in methane, producing aqueous methane and liquid

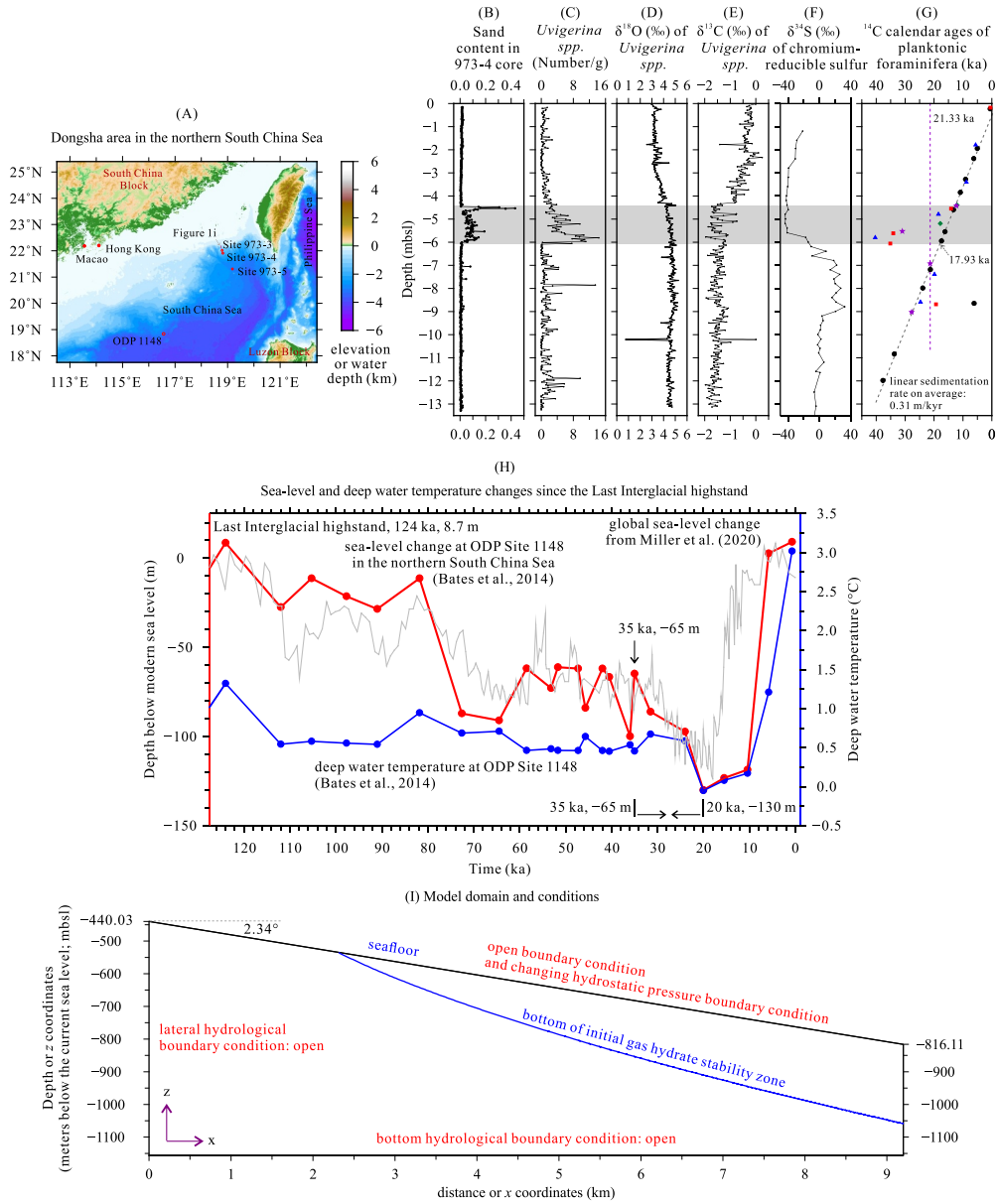

Figure 1. The background conditions and conceptualized model domain at the study site. (a) Map showing the location of the Dongsha area. Panels (b), (c), (d), (e) and (f) show the sand (grain diameter >0.063 mm) content, the number of *Uvigerina spp.*, the $\delta^{18}O$ values of *Uvigerina* spp., the $\delta^{13}C$ values of *Uvigerina* spp., and the $\delta^{34}S$ values of chromium-reducible sulfur in the 973–4 core, respectively (Huang et al., 2022). (g) The ^{14} C calendar ages of planktonic foraminifera in the 973–4 core (Lin et al., 2015; Shi et al., 2014; Zhang et al., 2015, 2018; Zhuang et al., 2015). (h) The red and blue lines show the sea level and deep water temperature changes, respectively, at ODP Site 1,148 since the last interglacial highstand (Bates et al., 2014). The gray line shows the global sea-level changes from Miller et al. (2020). (i) The conceptualized geometry of the two-dimensional model domain in the main simulations. In panels (a) and (i), the water depths are from the General Bathymetric Chart of the Oceans (GEBCO) 2020 bathymetry data set.

water. Dissociation occurs when the pressure–temperature–salinity conditions are no longer favorable for stable hydrates, producing gaseous methane and liquid water.

During the sea-level fall, there was hydrate dissociation at the BGHSZ and in the near-seafloor sediments near the upper limit of the GHSZ (Figures 2a or 2e). The hydrate dissociation at the shallow part of the BGHSZ was slightly less than that at the deep part of the BGHSZ (Figure 2a). The shallow BGHSZ was more influenced by the decrease in seafloor temperature from 35 to 20 ka (i.e., 0.5074°C) (Figure 1h), which inhibited hydrate

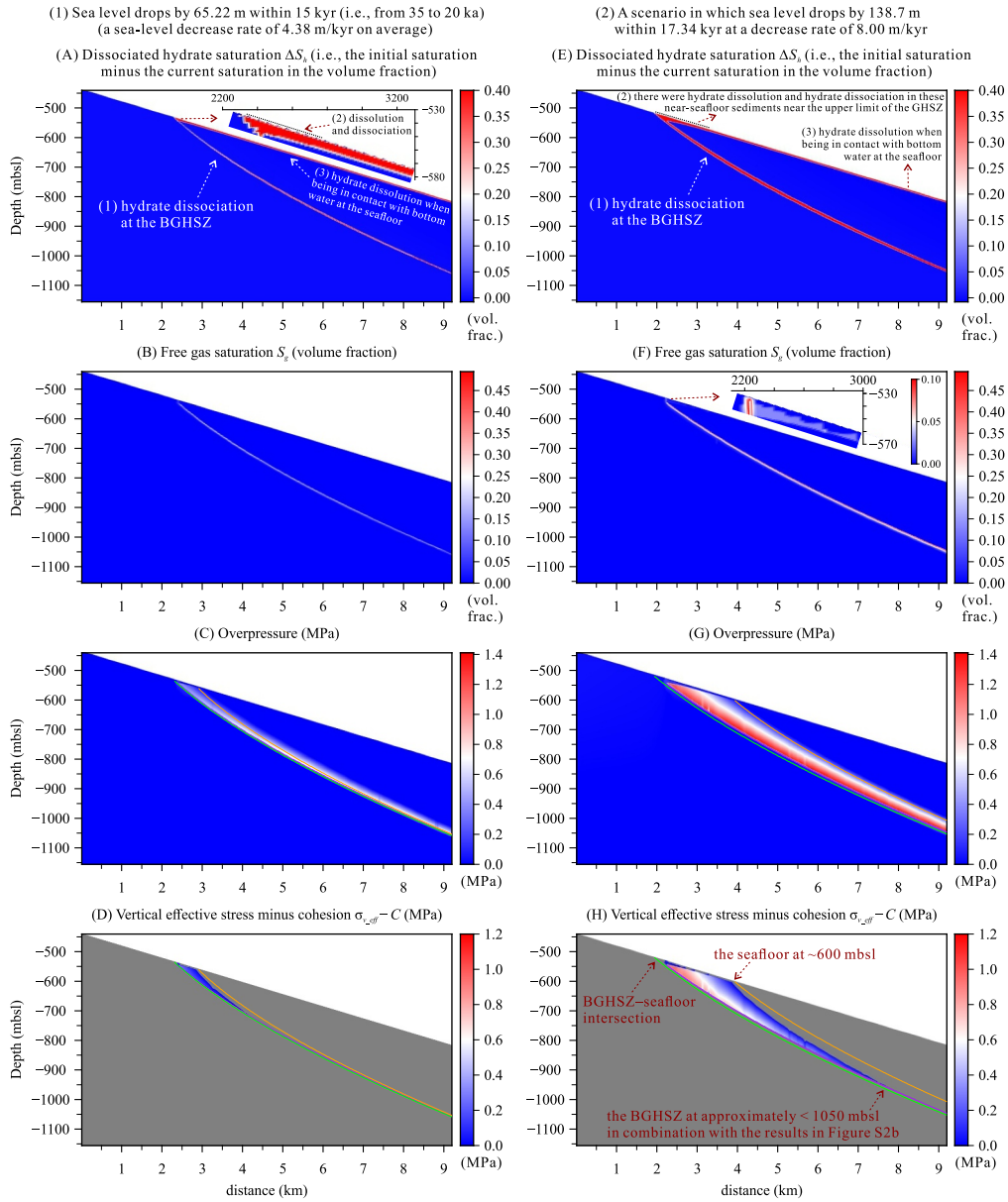

Figure 2. Modeled results from the main simulations. Positive values of the vertical effective stress minus cohesion ($\sigma_{v\_eff} - C > 0$) indicate the potential plastic deformation zone. The green, purple and orange lines in panels (c), (d), (g) and (h), and in Figures 3, 4 and Figure S4 in Supporting Information S1 indicate the locations of the initial BGHSZ, the modeled base of the hydrate zone after sea-level drops and the theoretical BGHSZ after sea-level drops (assuming that the temperatures are the same as the initial temperatures and that the pore pressure is hydrostatic), respectively. In panels (c) and (d), the locations of the purple lines are very close to those of the green lines. In panel (g), the location of the purple line is generally the same as that of the bottom boundary of the overpressure zone. In panels (d) and (h), the gray areas represent $\sigma_{v\_eff} - C \leq 0$.

dissociation. When this glacial decrease in temperature was not considered, the hydrate dissociation at the shallow BGHSZ was similar to that at the deep BGHSZ (Figure 2e). In the near-seafloor sediments near the upper limit of the GHSZ, sea-level and pressure drops could induce hydrate dissociation, and contact with the overlying hydrostatic ocean water facilitated overpressure dissipation (Figures 2c or 2g) and a shift in the boundary of the hydrate stability zone, which facilitated gradual hydrate dissociation toward increasing sediment depths and water depths with decreasing sea level (Figures 2a or 2e).

There was hydrate dissolution instead of dissociation at the seafloor (or below the sulfate–methane transition zone when hydrates were present below the sulfate–methane transition zone in nature) that was deeper than the upper

limit of the GHSZ (Figures 2a or 2e). Unless there was a sufficient methane supply from deep layers to form additional hydrates, this hydrate dissolution would occur constantly and gradually toward increasing sediment depths. A long contact time with bottom water induced considerable hydrate dissolution (Figure 2a). In the near-seafloor sediments near the upper limit of the GHSZ, there should be hydrate dissolution due to contact with bottom water before sea-level and pressure drops shifted the local system outside the hydrate stability zone, after which there should be hydrate dissociation.

Free gas occurred at the BGHSZ and in the near-seafloor sediments near the upper limit of the GHSZ due to hydrate dissociation because of sea-level drops. The maximum gas saturation was approximately 27.9% (Figure 2b).

Overpressure occurred at and above the BGHSZ (Figure 2c). The maximum overpressure was approximately 0.84 MPa. The vertical effective stress minus cohesion was positive at the tip of the GHSZ and at the shallow BGHSZ, where $z > -718.6$ m, indicating the potential plastic deformation zone ($\sigma_{v\_eff} - C > 0$; blue area in Figure 2d).

3.2. A Sea-Level Drop of 138.7 m at a Rate of 8.0 m/kyr

In this scenario, the results (Figures 2e–2h) were significantly greater than those resulting from a sea-level drop of 65.22 m (Figures 2a–2d). The maximum gas saturation reached 49.4% (Figure 2f). The maximum overpressure reached 1.41 MPa (Figure 2g). The accumulated overpressure at the BGHSZ and the endothermic character of hydrate dissociation tended to deepen the BGHSZ in return; thus, the shifted depths (i.e., the depth interval of hydrate dissociation) were smaller than the theoretical values. This was illustrated by the locations of the modeled base of the hydrate zone (purple lines in Figures 2c, 2d, 2g and 2h) and the theoretical BGHSZ (orange lines in Figures 2c, 2d, 2g and 2h) after sea-level drops. Therefore, this gas-hydrate system at the BGHSZ was likely a self-inhibited system (Liu & Flemings, 2009). The potential plastic deformation zone formed in the shallow part of the GHSZ and at the BGHSZ, where $z > -967.6$ m (Figure 2h).

Positive x-direction displacement (rightward) occurred near the initial GHSZ tip (i.e., the shallow end of the green line in Figure 3a), just beneath the shallow end of the modeled base of the hydrate zone (the purple line in Figure 3a), within the modeled hydrate zone where $z > -650.0$ m, and beneath the deep part of the modeled base of the hydrate zone where $x > 6{,}250$ m (Figure 3a). The maximum positive x-direction displacement was approximately 0.86 m at equilibrium. Negative x-direction displacement (leftward) occurred beneath the modeled base of the hydrate zone, where $x < 6{,}250$ m (Figure 3a).

The GHSZ exhibited generally positive z-direction displacement (upward) (Figures 3b and 4a). The near-seafloor area, which was within or just above the plastic deformation zone where $x < 3{,}250$ m, had great positive z-direction displacements (Figures 3b and 4a), indicating potentially significant sediment uplift or expansion. The maximum positive z-direction displacement was approximately 2.69 m at the aforementioned near-seafloor area at equilibrium. Negative z-direction displacement (downward) occurred beneath the modeled base of the hydrate zone, where $x < 7{,}750$ m (Figures 3b and 4a), resulting from the downward pressure from the overpressure just above the modeled base of the hydrate zone (Figure 2g).

Significant volumetric strain and shear strain occurred only at the top boundary (near-seafloor boundary) and bottom boundary (BGHSZ boundary) of the plastic deformation zone (Figures 3c and 3d).

4. Discussion

4.1. Likelihood of Glacial Hydrate Dissociation Causing Submarine Landslides

The significant positive x-direction displacement, positive z-direction displacement, volumetric strain and shear strain suggest that significant local plastic deformation could occur at the near-seafloor tip of the GHSZ (e.g., generally less than 1 km in length on the slope and less than 55 m below the local seafloor) (Figures 3a, 3d and 4a). That is, the mechanical displacements and related instability were limited to the hydrate zone at shallow water depths (Bryn et al., 2005). Moreover, the sediment plastic shear deformations should be confined to a short distance because of the stability and support of the downhill sediments above the BGHSZ, indicated by the negative or approximately zero x-direction displacements (leftward or approximately motionless in the horizontal direction) above the BGHSZ, where $x > 3{,}250$ m (Figures 3a and 4a).

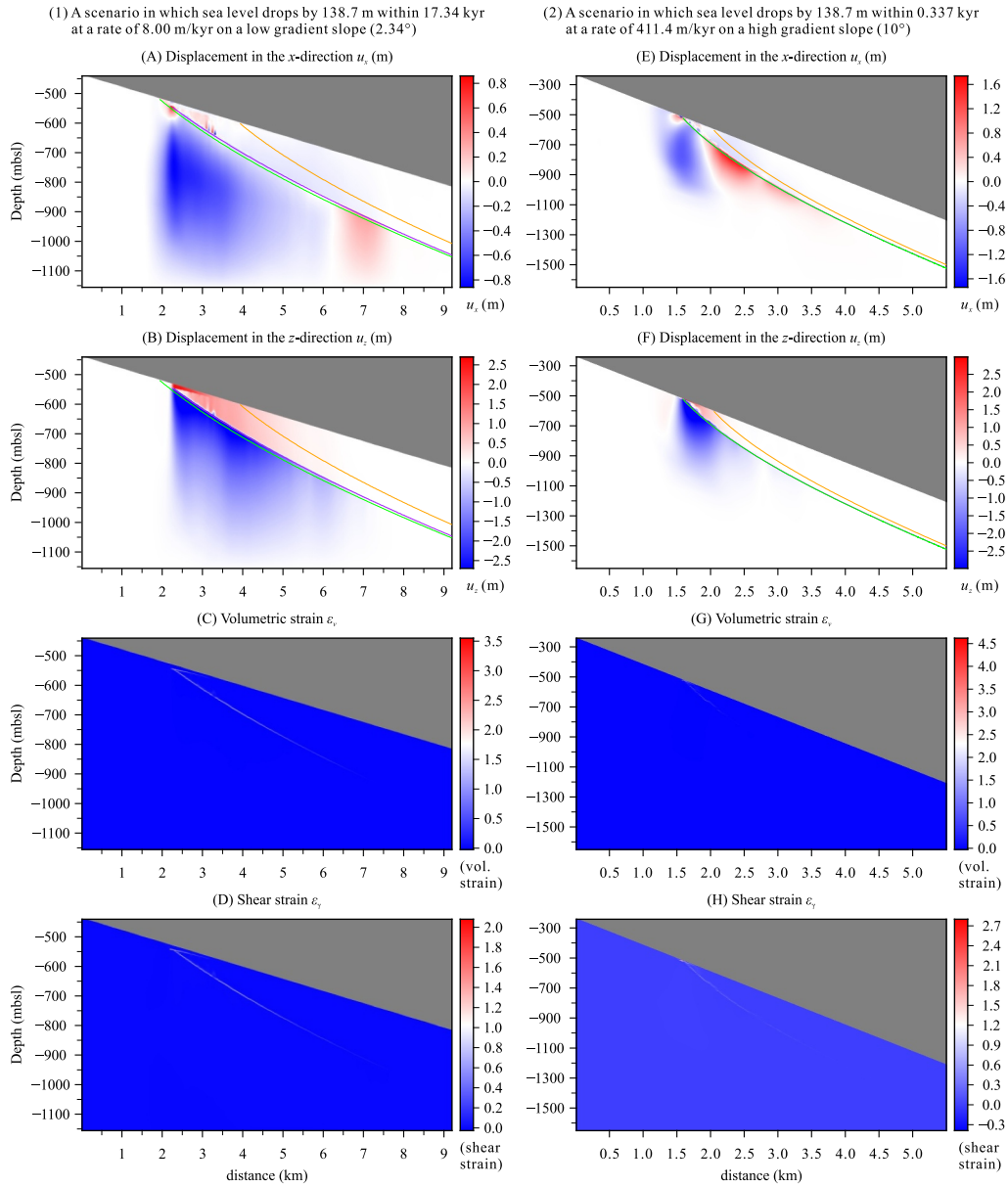

Figure 3. Modeled displacement and strain in two simulation scenarios. A positive (negative) *x*-direction displacement indicates rightward (leftward) displacement, and a positive (negative) *z*-direction displacement indicates upward (downward) displacement.

There should be a complete slip surface and significant relative displacement along the complete slip surface in a submarine landslide; that is, the displaced mass moves on a relatively thin zone of intense strain, that is, a slip surface (Locat & Lee, 2002; Talling et al., 2014). A slip surface is considered complete if it intersects both the upper and lower seafloor slopes, as illustrated in Figure 4a in Talling et al. (2014). As shown in Figures 3a–3d, there could be large deformation or local sliding along the BGHSZ boundary of the plastic deformation zone, as indicated by comparisons of the *x*-direction displacement across this boundary, the *z*-direction displacement across this boundary, and the significant volumetric and shear strain at this boundary. However, this potential slip surface was not a complete slip surface because it did not continue to extend and intersect the lower seafloor slope at an obtuse angle between the slip surface and the lower seafloor slope. This can be explained as follows. The bottom boundary of the plastic deformation zone is spatially similar to the BGHSZ, and the depth of the BGHSZ increases with increasing initial seafloor water depth on the slope. If the hydrate dissociation-induced overpressure is greater than the values estimated in this work, the bottom boundary of the plastic deformation zone

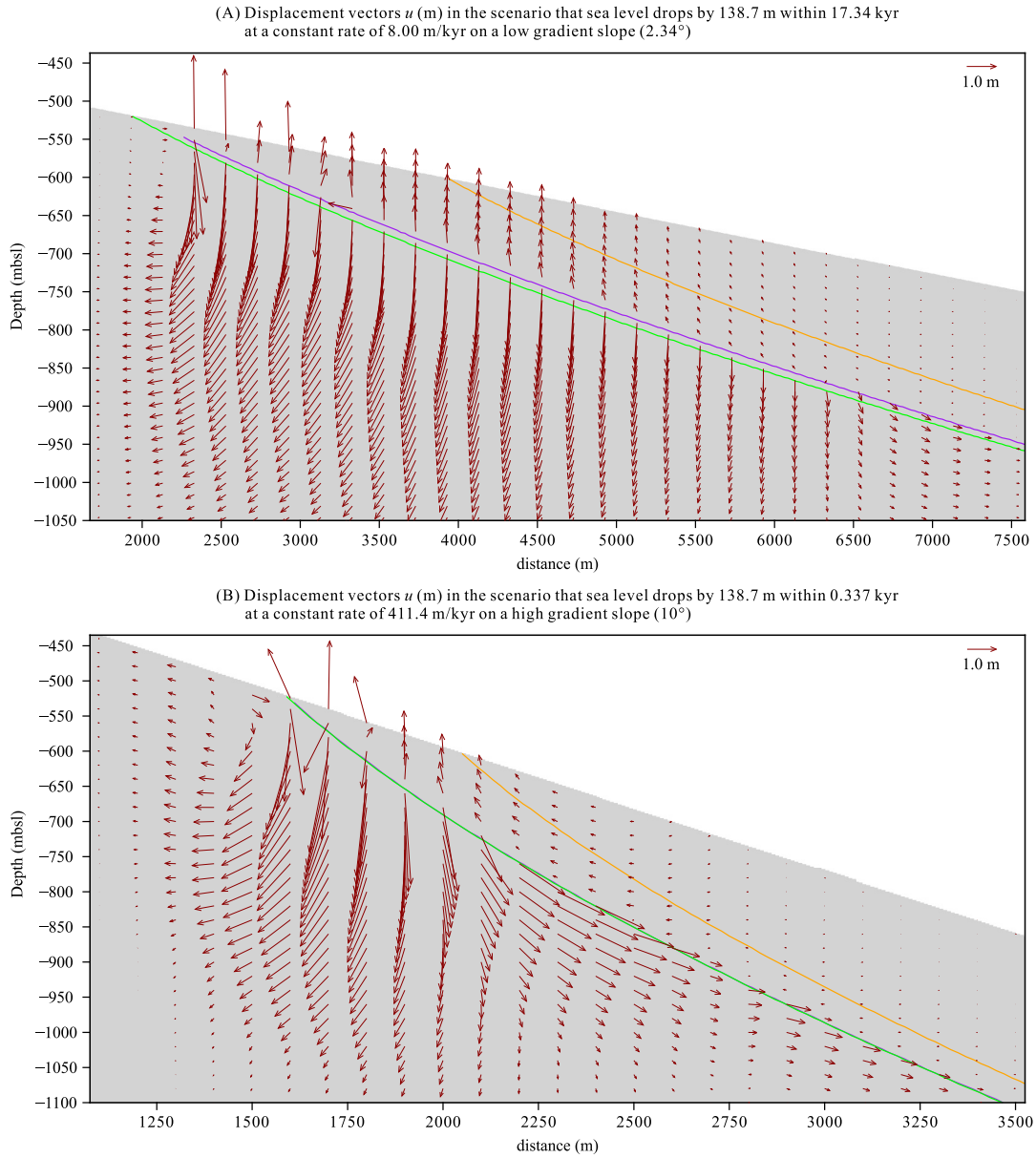

Figure 4. Modeled displacement vectors in two simulation scenarios. Panels (a) and (b) correspond to the displacement results in Figures 3a, 3b, 3e and 3f, respectively. The magnitudes of the vectors are directly proportional to the lengths of the vectors, and a length representing a magnitude of 1.0 m is shown in the upper right corners.

should extend toward greater depths rather than toward shallower sediment depths (mbsf) to intersect with the lower seafloor slope. Therefore, glacial hydrate dissociation was unlikely to form a complete slip surface or induce large-scale submarine landslides.

4.2. General Implications for the Possibility of Glacial Hydrate Dissociation Causing Submarine Landslides

The trends of our findings are representative of the general mechanisms that occur on marine hydrate-bearing slopes worldwide. This is supported as follows. First, the amplitudes of the sea-level drops in this work (Bates et al., 2014) are consistent with the global sea-level drops during the last glacial period (Miller et al., 2020) (Figure 1h). Therefore, the sea-level drop amplitudes in this work are representative of or comparable to those on marine hydrate-bearing slopes worldwide during the last glacial period. Second, a sensitivity analysis of the

model was conducted under various conditions, namely, sea-level drop rate, slope angle, initial hydrate distribution within the GHSZ and cohesion models of hydrate-bearing sediments, to include broad modeling scenarios and confirm the robustness of the broad conclusions. The small scale of the deformation at the near-seafloor tip of the GHSZ and the incompleteness of the potential slip surface (Section 4.1) remain unchanged even if there is a higher rate of sea-level drop (411.4 m/kyr) (Text S2 and Figures S2a, S2d and S2e in Supporting Information S1), a higher-angle slope (10°) (Figures 3e, 3h and 4b, S2b, S2d and S2e in Supporting Information S1), or a 50 m thick hydrate layer only above the BGHSZ at the initial time (Text S2 in Supporting Information S1). 411.4 m/kyr was the maximum sea-level drop rate (from 54.37 to 54.3 ka) during the last glacial period according to the global sea level data from Miller et al. (2020). As a result, sufficient sea-level drop amplitudes (65.22 or 138.7 m), sea-level drop rates (4.38 m/kyr on average, 8 m/kyr or 411.4 m/kyr) and slope angles (2.34° or 10°) are assessed. Notably, the aforementioned results and discussions (including Section 4.1) are based on low cohesion values for hydrate-bearing sediments ($C = 0.07 + 0.076S_h$(MPa); 0.07–0.1004 MPa for a hydrate saturation S_h from 0% to 40%) (Equation (3) in Text S1 in Supporting Information S1). For cohesions that were greater and likely more reasonable ($C = 0.28 + 2.0S_h$(MPa); 0.28–1.08 MPa for S_h from 0% to 40%) (Waite et al., 2009), the modeled plastic deformation zone could become too small to distinguish (Figures S2f, S2g and S2h in Supporting Information S1), let alone trigger sliding or large-scale submarine landslides.

The modeled water depths of the BGHSZ pinch-out zone (where the BGHSZ intersects the seafloor) in this work (520–535 mbsl) were similar to those in low-latitude regions globally, for example, 600 ± 50 mbsl on the Hikurangi margin (Mountjoy et al., 2014) and 515–520 mbsl at the Rio Grande Cone (Ketzer et al., 2020). The modeled extent of the potential plastic deformation zones should be more representative of those in low-latitude regions than those in high-latitude regions. This is because the BGHSZ pinch-out in high-latitude regions (e.g., 380–400 mbsl off Svalbard (Berndt et al., 2014)) was generally shallower than that in low-latitude regions, partly due to lower seafloor temperatures (e.g., approximately 3°C off Svalbard (Berndt et al., 2014)). In high-latitude regions, the potential plastic deformation zones should be in upper and shallower water regions due to their shallower BGHSZ pinch-outs. However, in both low-latitude and high-latitude regions, potential plastic deformation or slip is limited within the shallow-water region of the GHSZ, and the entire BGHSZ was not a complete slip surface due to a lack of slip along the deep portion of the BGHSZ (Figure S3d in Supporting Information S1).

4.3. Comparisons With Other Models and Field Evidence and Explanations of Observed Deep-Water Turbidites

Our results suggest that the gas pressure beneath the BGHSZ might exceed the overburden stress plus low cohesion values where the BGHSZ depth is shallower than 1,050 mbsl (Figure S2b in Supporting Information S1), supporting the case of an initial BGHSZ depth of approximately 925 mbsl in Liu and Flemings (2009). However, our two-dimensional modeling suggests that glacial hydrate dissociation alone was unlikely to form a complete slip surface and thus unlikely to induce large-scale slope failures. Instead, local instability (e.g., plastic strain) was more likely to occur in the GHSZ pinch-out zone (Figures 3 and 4). This local instability is consistent with field observations showing that the landward edge of creeping coincides with the BGHSZ pinch-out at the seafloor (600 ± 50 mbsl) in the Tuaheni Landslide Complex (Pecher et al., 2018). Mountjoy et al. (2014) showed that there could be compressional deformation in the upper slide debris region and extensional deformation in the lower slide debris region separated by the BGHSZ pinch-out in hydrate-controlled plastic deformation structures according to seismic reflection and bathymetry data. Our simulations produced compression (small blue areas surrounded by red areas in Figures 3a and 3e) and extension zones (red areas in Figures 3a and 3e) in the GHSZ pinch-out zone. The local instability in the GHSZ pinch-out zone might be somewhat enhanced when coinciding with the pressure release (up to several bars) during burial-driven gas hydrate recycling (Gupta et al., 2023). The GHSZ pinch-out zone is an important area for investigating overpressure and focused fluid flow (Figure S4), localized plastic deformation or slip, or downslope sediment transport related to glacial hydrate dissociation (e.g., Daigle et al., 2020; Flemings, 2021; Mountjoy et al., 2014; Pecher et al., 2018; Priest & Grozic, 2016; You et al., 2022).

The observed turbidite deposits occurred at a wide range of seafloor water depths, for example, 1,026–2,998 mbsl near our study site (2.45–8.5 mbsf) (Chen et al., 2014; Huang et al., 2022) and 750–4,500 mbsl on the southern Carolina Rise and inner Blake Ridge (approximately 2 mbsf) (Paull et al., 1996). That is, the observed turbidite deposits formed at water depths that could be too deep or too far from the GHSZ pinch-out zone (e.g., <600 mbsl) (Hühnerbach et al., 2004; Talling et al., 2014). The deep-water (much greater than 600 mbsl) area was unlikely to

have experienced plastic creep due to hydrate dissociation or was directly influenced by plastic creep locally at the GHSZ tip area. In fact, there could be seafloor erosion of uplifted or expanded ridges close to the GHSZ pinch-out zone (Pecher et al., 2005) or downslope movement of detached materials from the GHSZ pinch-out zone (Mountjoy et al., 2014). That is, erosion and detachment from the GHSZ pinch-out zone, which was deformed (e.g., uplifted or expanded) by glacial hydrate dissociation (Figures 3b, 3f and 4), could have occurred. This may be one of the potential mechanisms (Elger et al., 2018; Lee, 2009; Talling et al., 2014) explaining the occurrence of thin layers of deep-water (much greater than 600 mbsl) turbidite containing geochemical evidence of glacial hydrate dissociation (Figures 1c–1f) in marine gas hydrate fields worldwide.

5. Conclusions

Our simulations suggest that glacial hydrate dissociation might induce plastic deformation or slip only possibly in the shallow-water region of the GHSZ. This region is generally smaller than the area enclosed by three points, that is, the BGHSZ–seafloor intersection, the seafloor at ∼600 mbsl and the BGHSZ at ∼1,050 mbsl in low-latitude regions. The GHSZ pinch-out zone and the shallow part (<1,050 mbsl) of the BGHSZ might slip at localized and small scales. The deep part (>1,050 mbsl) of the BGHSZ could not slip; therefore, the entire BGHSZ was not a complete slip surface. Glacial hydrate dissociation alone was unlikely to trigger large-scale submarine landslides. The observed deep-water (much greater than 600 mbsl) turbidites containing geochemical evidence of glacial hydrate dissociation might have been eroded or detached from the GHSZ pinch-out zone deformed (e.g., uplifted or expanded) by glacial hydrate dissociation.

Conflict of Interest

The authors declare no conflicts of interest relevant to this study.

Data Availability Statement

The source data, modeling data and code used in this study are listed in the references (Bates et al., 2014; Huang et al., 2022; Miller et al., 2020) or available in Liu et al. (2024).

Acknowledgments
This work was supported by the National Natural Science Foundation of China (42006179, 41576035, 42006071), the Basic and Applied Basic Research Foundation of Guangdong Province (2021A1515010686), and the Special Fund of the South China Sea Institute of Oceanology of the Chinese Academy of Sciences (SCSIO2023QY06). Shubhangi Gupta was supported by the MSCA Postdoctoral ERA Fellowships 2021 action, under the Horizon Europe program, project 'WarmArctic', number 101090338. Contributions from the Lawrence Berkeley National Laboratory were supported by the U.S. Department of Energy under contract DE-AC02-05CH11231. The authors gratefully acknowledge Christian Huber and two anonymous reviewers for their constructive comments on the manuscript.

References

Bates, S. L., Siddall, M., & Waelbroeck, C. (2014). Hydrographic variations in deep ocean temperature over the mid-Pleistocene transition. *Quaternary Science Reviews*, *88*, 147–158. https://doi.org/10.1016/j.quascirev.2014.01.020

Berndt, C., Feseker, T., Treude, T., Krastel, S., Liebetrau, V., Niemann, H., et al. (2014). Temporal constraints on hydrate-controlled methane seepage off Svalbard. *Science*, *343*(6168), 284–287. https://doi.org/10.1126/science.1246298

Bryn, P., Berg, K., Forsberg, C. F., Solheim, A., & Kvalstad, T. J. (2005). Explaining the storegga slide. *Marine and Petroleum Geology*, *22*(1), 11–19. https://doi.org/10.1016/j.marpetgeo.2004.12.003

Chen, F., Zhuang, C., Zhang, G., Lu, H., Duan, X., Zhou, Y., et al. (2014). Abnormal sedimentary events and gas hydrate dissociation in Dongsha area of the South China sea during last glacial period. *Earth Science - Journal of China University of Geosciences*, *39*(11), 1517–1526. https://doi.org/10.3799/dqkx.2014.144

Daigle, H., Cook, A., Fang, Y., Bihani, A., Song, W., & Flemings, P. B. (2020). Gas-driven tensile fracturing in shallow marine sediments. *Journal of Geophysical Research: Solid Earth*, *125*(12), 1–19. https://doi.org/10.1029/2020JB020835

Elger, J., Berndt, C., Rüpke, L., Krastel, S., Gross, F., & Geissler, W. H. (2018). Submarine slope failures due to pipe structure formation. *Nature Communications*, *9*, 1–6. https://doi.org/10.1038/s41467-018-03176-1

Flemings, P. B. (2021). *A concise guide to geopressure: Origin, prediction, and applications*. Cambridge University Press. https://doi.org/10.1017/9781107326309

Gupta, S., Burwicz-Galerne, E., Schmidt, C., & Rüpke, L. (2023). Periodic states and their implications in gas hydrate systems. *Earth and Planetary Science Letters*, *624*, 118445. https://doi.org/10.1016/j.epsl.2023.118445

Handwerger, A. L., Rempel, A. W., & Skarbek, R. M. (2017). Submarine landslides triggered by destabilization of high-saturation hydrate anomalies. *Geochemistry, Geophysics, Geosystems*, *18*(7), 2429–2445. https://doi.org/10.1002/2016GC006706

Huang, Y., Cheng, J., Wang, M., Wang, S., & Yan, W. (2022). Gas hydrate dissociation events during LGM and their potential trigger of submarine landslides: Foraminifera and geochemical records from two cores in the northern South China sea. *Frontiers in Earth Science*, *10*, 1–11. https://doi.org/10.3389/feart.2022.876913

Hühnerbach, V., Masson, D. G., & Partners of the COSTA-Project. (2004). Landslides in the north atlantic and its adjacent seas: An analysis of their morphology, setting and behaviour. *Marine Geology*, *213*(1–4), 343–362. https://doi.org/10.1016/j.margeo.2004.10.013

Ketzer, M., Praeg, D., Rodrigues, L. F., Augustin, A., Pivel, M. A. G., Rahmati-Abkenar, M., et al. (2020). Gas hydrate dissociation linked to contemporary ocean warming in the southern hemisphere. *Nature Communications*, *11*, 1–9. https://doi.org/10.1038/s41467-020-17289-z

Lee, H. J. (2009). Timing of occurrence of large submarine landslides on the Atlantic Ocean margin. *Marine Geology*, *264*(1–2), 53–64. https://doi.org/10.1016/j.margeo.2008.09.009

Lin, Q., Wang, J., Fu, S., Lu, H., Bu, Q., Lin, R., & Sun, F. (2015). Elemental sulfur in northern South China Sea sediments and its significance. *Science China Earth Sciences*, *58*(12), 2271–2278. https://doi.org/10.1007/s11430-015-5182-7

Liu, J., Gupta, S., Rutqvist, J., Ma, Y., Wang, S., Wan, K., et al. (2024). Data associated with the manuscript: Can glacial sea-level drop-induced gas hydrate dissociation cause submarine landslides? (Version 4) [Dataset]. *Figshare*. https://doi.org/10.6084/m9.figshare.22598236.v4

Liu, X., & Flemings, P. (2009). Dynamic response of oceanic hydrates to sea level drop. *Geophysical Research Letters*, *36*(17), 1–5. https://doi.org/10.1029/2009GL039821

Liu, Z., Dai, S., Ning, F., Peng, L., Wei, H., & Wei, C. (2018). Strength estimation for hydrate-bearing sediments from direct shear tests of hydrate-bearing sand and silt. *Geophysical Research Letters*, *45*(2), 715–723. https://doi.org/10.1002/2017GL076374

Locat, J., & Lee, H. J. (2002). Submarine landslides: Advances and challenges. *Canadian Geotechnical Journal*, *39*(1), 193–212. https://doi.org/10.1139/t01-089

Maslin, M., Mikkelsen, N., Vilela, C., & Haq, B. (1998). Sea-level –and gas-hydrate–controlled catastrophic sediment failures of the Amazon Fan. *Geology*, *26*(12), 1107–1110. https://doi.org/10.1130/0091-7613(1998)026%3C1107:SLAGHC%3E2.3.CO;2

Maslin, M., Vilela, C., Mikkelsen, N., & Grootes, P. (2005). Causes of catastrophic sediment failures of the Amazon Fan. *Quaternary Science Reviews*, *24*(20–21), 2180–2193. https://doi.org/10.1016/j.quascirev.2005.01.016

Miller, K. G., Browning, J. V., Schmelz, W. J., Kopp, R. E., Mountain, G. S., & Wright, J. D. (2020). Cenozoic sea-level and cryospheric evolution from deep-sea geochemical and continental margin records. *Science Advances*, *6*(20), 1–15. https://doi.org/10.1126/sciadv.aaz1346

Moridis, G. J. (2014). *User's manual for the HYDRATE v1.5 option of TOUGH+v1.5: A code for the simulation of system behavior in hydrate-bearing geologic media. (Rep. LBNL-6869E)*. Lawrence Berkeley National Laboratory.

Mountjoy, J. J., Pecher, I., Henrys, S., Crutchley, G., Barnes, P. M., & Plaza-Faverola, A. (2014). Shallow methane hydrate system controls ongoing, downslope sediment transport in a low-velocity active submarine landslide complex, Hikurangi Margin, New Zealand. *Geochemistry, Geophysics, Geosystems*, *15*(11), 4137–4156. https://doi.org/10.1002/2014GC005379

Nixon, M. F., & Grozic, J. L. (2007). Submarine slope failure due to gas hydrate dissociation: A preliminary quantification. *Canadian Geotechnical Journal*, *44*(3), 314–325. https://doi.org/10.1139/t06-121

Owen, M., Day, S., & Maslin, M. (2007). Late pleistocene submarine mass movements: Occurrence and causes. *Quaternary Science Reviews*, *26*(7–8), 958–978. https://doi.org/10.1016/j.quascirev.2006.12.011

Paull, C. K., Buelow, W. J., Ussler, W., III, & Borowski, W. S. (1996). Increased continental-margin slumping frequency during sea-level lowstands above gas hydrate–bearing sediments. *Geology*, *24*(2), 143–146. https://doi.org/10.1130/0091-7613(1996)024<0143:ICMSFD>2.3.CO;2

Paull, C. K., Ussler, W., & Dillon, W. P. (2003). Potential role of gas hydrate decomposition in generating submarine slope failures. In M. D. Max (Ed.), *Natural gas hydrate: In oceanic and permafrost environments* (Vol. 5, pp. 149–156). Springer. https://doi.org/10.1007/978-94-011-4387-5_12

Pecher, I. A., Barnes, P. M., & LeVay, L. J., & the Expedition 372 Scientists. (2018). *Expedition 372 preliminary report: Creeping gas hydrate slides and Hikurangi LWD*. International Ocean Discovery Program. https://doi.org/10.14379/iodp.pr.372.2018

Pecher, I. A., Henrys, S. A., Ellis, S., Chiswell, S. M., & Kukowski, N. (2005). Erosion of the seafloor at the top of the gas hydrate stability zone on the Hikurangi Margin, New Zealand. *Geophysical Research Letters*, *32*(24), 1–4. https://doi.org/10.1029/2005GL024687

Priest, J. A., & Grozic, J. L. H. (2016). Stability of fine-grained sediments subject to gas hydrate dissociation in the Arctic continental margin. In G. Lamarche, J. Mountjoy, S. Bull, T. Hubble, S. Krastel, E. Lane, et al. (Eds.), *Submarine mass movements and their consequences* (Vol. 41, pp. 427–436). Springer International Publishing. https://doi.org/10.1007/978-3-319-20979-1_43

Reagan, M. T., Moridis, G. J., Elliott, S. M., & Maltrud, M. (2011). Contribution of oceanic gas hydrate dissociation to the formation of Arctic Ocean methane plumes. *Journal of Geophysical Research*, *116*(C9), 1–11. https://doi.org/10.1029/2011JC007189

Shi, C., Lei, H., Zhao, J., Zhang, J., & Han, C. (2014). Vertical microbial community structure characteristics of sediment in gas hydrate potential area of northern South China sea jiulong methane reef. *Acta Sedimentologica Sinica*, *32*(6), 1072–1082. http://www.cjxb.ac.cn/en/article/id/3471

Sultan, N., Cochonat, P., Foucher, J. P., & Mienert, J. (2004). Effect of gas hydrates melting on seafloor slope instability. *Marine Geology*, *213*(1–4), 379–401. https://doi.org/10.1016/j.margeo.2004.10.015

Talling, P., Clare, M., Urlaub, M., Pope, E., Hunt, J., & Watt, S. (2014). Large submarine landslides on continental slopes: Geohazards, methane release, and climate change. *Oceanography*, *27*(2), 32–45. https://doi.org/10.5670/oceanog.2014.38

Waite, W. F., Santamarina, J. C., Cortes, D. D., Dugan, B., Espinoza, D. N., Germaine, J., et al. (2009). Physical properties of hydrate-bearing sediments. *Reviews of Geophysics*, *47*(4), 1–38. https://doi.org/10.1029/2008RG000279

You, K., Flemings, P., Bhandari, A. R., Heidari, M., & Germaine, J. (2022). The role of creep in geopressure development. *Petroleum Geoscience*, *28*(3), 1–12. https://doi.org/10.1144/petgeo2021-064

Zhang, B., Pan, M., Wu, D., & Wu, N. (2018). Distribution and isotopic composition of foraminifera at cold-seep Site 973-4 in the Dongsha area, northeastern South China Sea. *Journal of Asian Earth Sciences*, *168*, 145–154. https://doi.org/10.1016/j.jseaes.2018.05.007

Zhang, B., Wu, D., & Wu, N. (2015). Characteristics of sedimentary geochemistry and their responses to cold-seep activities in Dongsha, the northern South China Sea. *Marine Geology Frontiers*, *31*(9), 14–27. https://doi.org/10.16028/j.1009-2722.2015.09003

Zhuang, C., Chen, F., Cheng, S., Lu, H., Zhou, Y., & Liu, G. (2015). Stable isotopic characteristics and their influencing factors of benthic foraminifera in the prospective gas hydrate area from the northern South China Sea since the last glacial. *Quaternary Sciences*, *35*(2), 422–432. http://www.dsjyj.com.cn/CN/article/downloadArticleFile.do?attachType=PDF&id=11027

References From the Supporting Information

Athy, L. F. (1930). Density, porosity, and compaction of sedimentary rocks. *AAPG Bulletin*, *14*(1), 1–24. https://doi.org/10.1306/3D93289E-16B1-11D7-8645000102C1865D

Cloetingh, S., van Wees, J. D., Ziegler, P. A., Lenkey, L., Beekman, F., Tesauro, M., et al. (2010). Lithosphere tectonics and thermo-mechanical properties: An integrated modelling approach for Enhanced Geothermal Systems exploration in Europe. *Earth-Science Reviews*, *102*(3–4), 159–206. https://doi.org/10.1016/j.earscirev.2010.05.003

Daigle, H., & Dugan, B. (2010). Origin and evolution of fracture-hosted methane hydrate deposits. *Journal of Geophysical Research: Solid Earth (1978–2012)*, *115*(B11), 1–21. https://doi.org/10.1029/2010JB007492

Garg, S. K., Pritchett, J. W., Katoh, A., Baba, K., & Fujii, T. (2008). A mathematical model for the formation and dissociation of methane hydrates in the marine environment. *Journal of Geophysical Research*, *113*(B1), B01201. https://doi.org/10.1029/2006JB004768

Gupta, S., Helmig, R., & Wohlmuth, B. (2015). Non-isothermal, multi-phase, multi-component flows through deformable methane hydrate reservoirs. *Computational Geosciences*, *19*(5), 1063–1088. https://doi.org/10.1007/s10596-015-9520-9

Haacke, R. R., Westbrook, G. K., & Riley, M. S. (2008). Controls on the formation and stability of gas hydrate-related bottom-simulating reflectors (BSRs): A case study from the west svalbard continental slope. *Journal of Geophysical Research*, *113*(B5), B05104. https://doi.org/10.1029/2007JB005200

Heeschen, K. U., Collier, R. W., de Angelis, M. A., Suess, E., Rehder, G., Linke, P., & Klinkhammer, G. P. (2005). Methane sources, distributions, and fluxes from cold vent sites at Hydrate Ridge, Cascadia Margin. *Global Biogeochemical Cycles*, *19*(2), 1–19. https://doi.org/10.1029/2004GB002266

Kossel, E., Deusner, C., Bigalke, N., & Haeckel, M. (2018). The dependence of water permeability in quartz sand on gas hydrate saturation in the pore space. *Journal of Geophysical Research: Solid Earth*, *123*(2), 1235–1251. https://doi.org/10.1002/2017JB014630

Liao, W.-Z., Lin, A. T., Liu, C.-S., Oung, J.-N., & Wang, Y. (2014). Heat flow in the rifted continental margin of the South China Sea near Taiwan and its tectonic implications. *Journal of Asian Earth Sciences*, *92*, 233–244. https://doi.org/10.1016/j.jseaes.2014.01.003

Liu, X., & Flemings, P. B. (2007). Dynamic multiphase flow model of hydrate formation in marine sediments. *Journal of Geophysical Research*, *112*(B3), B03101. https://doi.org/10.1029/2005JB004227

Liu, X., & Flemings, P. B. (2011). Capillary effects on hydrate stability in marine sediments. *Journal of Geophysical Research*, *116*(B7), B07102. https://doi.org/10.1029/2010JB008143

Mahabadi, N., Dai, S., Seol, Y., Sup Yun, T., & Jang, J. (2016). The water retention curve and relative permeability for gas production from hydrate-bearing sediments: Pore-network model simulation. *Geochemistry, Geophysics, Geosystems*, *17*(8), 3099–3110. https://doi.org/10.1002/2016GC006372

Mahabadi, N., & Jang, J. (2014). Relative water and gas permeability for gas production from hydrate-bearing sediments. *Geochemistry, Geophysics, Geosystems*, *15*(6), 2346–2353. https://doi.org/10.1002/2014GC005331

Masui, A., Haneda, H., Ogata, Y., & Aoki, K. (2005). The effect of saturation degree of methane hydrate on the shear strength of synthetic methane hydrate sediments. In *Paper presented at 5th international conference on gas hydrates (ICGH5), trondheim, Norway*.

Masui, A., Haneda, H., Ogata, Y., & Aoki, K. (2006). Triaxial compression test on submarine sediment containing methane hydrate in deep sea off the coast of Japan (in Japanese). In *Paper presented at the 41st annual conference, Japanese geotechnical society, kagoshima, Japan, 12–14 july*.

Neuzil, C. (1994). How permeable are clays and shales? *Water Resources Research*, *30*(2), 145–150. https://doi.org/10.1029/93WR02930

Rutqvist, J., & Moridis, G. J. (2009). Numerical studies on the geomechanical stability of hydrate-bearing sediments. *SPE Journal, SPE-126129-PA*, *14*(02), 267–282. https://doi.org/10.2118/126129-PA

Sarkar, S., Berndt, C., Minshull, T. A., Westbrook, G. K., Klaeschen, D., Masson, D. G., et al. (2012). Seismic evidence for shallow gas-escape features associated with a retreating gas hydrate zone offshore west Svalbard. *Journal of Geophysical Research*, *117*(B9), B09102. https://doi.org/10.1029/2011JB009126

Smith, A. J., Flemings, P. B., Liu, X., & Darnell, K. (2014). The evolution of methane vents that pierce the hydrate stability zone in the world's oceans. *Journal of Geophysical Research: Solid Earth*, *119*(8), 6337–6356. https://doi.org/10.1002/2013JB010686

Song, H., Geng, J., Wang, H., Zhang, W., Fang, Y., Hao, T., & Jiang, W. (2001). A preliminary study of gas hydrates in Dongsha region north of South China Sea. *Chinese Journal of Geophysics*, *44*(5), 684–691. https://doi.org/10.1002/cjg2.187

Stone, H. L. (1970). Probability model for estimating three-phase relative permeability. *Journal of Petroleum Technology*, *22*(02), 214–218. https://doi.org/10.2118/2116-PA

Van Genuchten, M. T. (1980). A closed-form equation for predicting the hydraulic conductivity of unsaturated soils. *Soil Science Society of America Journal*, *44*(5), 892–898. https://doi.org/10.2136/sssaj1980.03615995004400050002x

Wang, L., Sun, X., Shen, S., Wu, P., Liu, T., Liu, W., et al. (2020). Undrained triaxial tests on water-saturated methane hydrate–bearing clayey-silty sediments of the South China Sea. *Canadian Geotechnical Journal*, *58*(3), 351–366. https://doi.org/10.1139/cgj-2019-0711

Westbrook, G. K., Thatcher, K. E., Rohling, E. J., Piotrowski, A. M., Pälike, H., Osborne, A. H., et al. (2009). Escape of methane gas from the seabed along the West Spitsbergen continental margin. *Geophysical Research Letters*, *36*(15), L15608. https://doi.org/10.1029/2009GL039191

Yang, X., Shi, X., Zhao, J., Yu, C., Gao, H., Chen, A., et al. (2018). Bottom water temperature measurements in the South China sea, eastern Indian ocean and western pacific ocean. *Journal of Tropical Oceanography*, *37*(5), 86–97. https://doi.org/10.11978/2017113

Yang, Y., & Lei, H. (2016). Geochemical characteristics of carbon in core 973-4 from southwestern Taiwan Basin in northern South China Sea. *Marine Sciences*, *40*(8), 100–107. http://qdhys.ijournal.cn/hykx/ch/reader/create_pdf.aspx?file_no=20160814&flag=1&journal_id=hykx&year_id=2016

Yuan, Y., Zhu, W., Mi, L., Zhang, G., Hu, S., & He, L. (2009). "Uniform geothermal gradient" and heat flow in the qiongdongnan and pearl river mouth basins of the South China sea. *Marine and Petroleum Geology*, *26*(7), 1152–1162. https://doi.org/10.1016/j.marpetgeo.2008.08.008